Nanoscale

PAPER

View Article Online
View Journal | View Issue

Cite this: *Nanoscale*, 2015, **7**, 8566

Facile production of stable silicon nanoparticles: laser chemistry coupled to *in situ* stabilization *via* room temperature hydrosilylation†

A. Malumbres,[a,b] G. Martínez,*[a,b] J. L. Hueso,[a,b] J. Gracia,[a] R. Mallada,[a,b] A. Ibarra[c] and J. Santamaría*[a,b]

Received 12th February 2015,
Accepted 3rd April 2015

DOI: 10.1039/c5nr01031d

www.rsc.org/nanoscale

Stable, alkyl-terminated, light-emitting silicon nanoparticles have been synthesized in a continuous process by laser pyrolysis of a liquid trialkyl-silane precursor selected as a safer alternative to gas silane (SiH_4). Stabilization was achieved by *in situ* reaction using a liquid collection system instead of the usual solid state filtration. The alkene contained in the collection liquid (1-dodecene) reacted with the newly formed silicon nanoparticles in an unusual room-temperature hydrosilylation process. It was achieved by the presence of fluoride species, also produced during laser pyrolysis from the decomposition of sulfur hexafluoride (SF_6) selected as a laser sensitizer. This process directly rendered alkyl-passivated silicon nanoparticles with consistent morphology and size (<3 nm), avoiding the use of costly post-synthetic treatments.

Introduction

Silicon nanoparticles (Si NPs) have been heralded as outstanding materials for technological applications in photovoltaic and microelectronic devices[1–3] on account of their optical properties and the richness of their surface chemistry.[4,5] The fact that Si NPs are biodegradable[6–8] has enabled additional opportunities in environmental/health related applications.[9] However, the fabrication of Si NPs with the required characteristics and long-term stability represents a formidable challenge to synthetic chemists since, in order to display efficient visible photoluminescence (PL) based on band gap emission, Si NPs must be smaller than 5 nm, and their surface must be "properly passivated".[10]

The preparation of Si NPs can be typically defined as a two-stage process: (i) synthesis of the crystalline Si cores and (ii) surface-capping/passivation. Top down processes to produce luminescent surface-capped Si NPs include laser ablation of bulk silicon targets,[11–15] microwave heating of nanowires[16] or mechano-chemical-based[17] treatments. However, these methods generally face the major drawback of an intrinsically wide size distribution of the produced nanoparticles.[18] Furthermore, extended aging times,[17,19] or post-treatment with strong acids such as hydrofluoric acid (HF) to remove the amorphous and oxidized shell[20] are needed to obtain luminescent silicon nanocrystals. In contrast, bottom-up approaches may be preferred given the higher control of size and shape distributions.[21] Bottom-up methods to fabricate stable silicon colloids generally require liquid-phase synthesis in the presence of coordinating ligands. For instance, successful synthesis routes have been demonstrated in micelle systems[10,22,23] and melt procedures,[24,25] based on the NH_4Br metathesis of a Zintl salt. However, wet chemistry synthesis for silicon also requires extended reaction times (up to 20 h) and yields small quantities of crystalline material due to the limited range of temperatures accessible in the presence of liquid solvents. In addition, tedious purification processes are required.[22,26] Other bottom-up approaches based on laser pyrolysis[27–29] or non-thermal plasma reactors[30,31] have also demonstrated the capability of generating silicon nanocrystals from the gaseous phase and their subsequent functionalization with organic ligands in a second step conducted in the liquid phase. Unfortunately, these methods suffer from important limitations such as the use of highly toxic flammable silane (SiH_4)[28,31] which is conventionally used as a gas precursor and the fact that nanoparticles (typically collected in a filter at the reactor outlet) are often clustered into large aggregates, which may annihilate the desired quantum confinement properties. Therefore, a preliminary etching step is generally required to achieve effective yields of photoluminescence[28] prior to the liquid-phase functionalization step.

[a]*Networking Research Center on Bioengineering, Biomaterials and Nanomedicine, CIBER-BBN, 28029 Madrid, Spain*
[b]*Department of Chemical Engineering, Nanoscience Institute of Aragon (INA), Universidad de Zaragoza, 50018 Zaragoza, Spain.*
E-mail: jesus.santamaria@unizar.es, gemamar@unizar.es; Tel: +34 976761153
[c]*Advanced Microscopy Laboratory (LMA), Nanoscience Institute of Aragon (INA), 50018 Zaragoza, Spain*
†Electronic supplementary information (ESI) available. See DOI: 10.1039/c5nr01031d

Herein, we have developed an integrated bottom-up process to obtain stabilized, fluorescent silicon nanocrystals. Our synthesis strategy uses laser pyrolysis to decompose a safer silicon precursor and produce Si nanocrystals of suitable size. Hence, hydrosilylation to obtain stable alkyl-terminated silicon nanoparticles has been carried out on a single on-line liquid (dodecene) collection/functionalization step at room temperature. This is a highly demanding task, considering that room temperature hydrosilylation must be obtained in the short residence time of the gas bubbles within the collection flask. In addition, we show that the process can be facilitated by the residual fluoride anions resulting from the decomposition of the laser sensitizer (SF_6) in a role similar to that reported for residual fluoride from HF etching. Thus alkyl-stabilized photoluminescent silicon nanoparticles are obtained in a simple, continuous fashion.

The method presented here represents a significant improvement with respect to previously reported laser pyrolysis syntheses, on account of several facts: (i) a greener molecule (dimethylethylsilane) as a liquid silicon precursor, instead of the highly toxic and flammable gas silane (SiH_4) is used; (ii) the process directly yields a stable dispersion of crystalline Si nanoparticles with a diameter under 3 nm, thus avoiding costly post-synthetic treatments (acid etching to reduce the particle size or partial dissolution and sonication to redisperse particulate agglomerates); (iii) the liquid collection system used allows the implementation of a continuous process for Si nanoparticle production and stabilization.

Experimental section

Chemicals

Dimethylethylsilane (DMES, 98%), 1-dodecene (95%), ethylaluminium chloride solution in hexane (1.0 M), absolute ethanol (≥98%) and deuterated chloroform ($CHCl_3$-d1 99.8% D) were purchased from Sigma Aldrich. To avoid the contribution of solvent impurities to fluorescence, dodecene was purified with active carbon for 12 hours. To circumvent further oxidation of the silicon nanoparticles oxygen and water were removed from the solvent before the reaction. Dodecene was first deaerated followed by distillation at reduced pressure and stored over molecular sieves under an inert atmosphere.

Nanoparticle synthesis and collection

The laser pyrolysis reactor and the liquid collection system used in this work have been described elsewhere.[32,33] In this case, dimethylethylsilane (DMES) stored in a sealed glass reservoir at 0 °C was the silicon precursor. A stream of 2 sccm of the carrier gas sulphur hexafluoride (SF_6) was bubbled into the precursor container to feed it at the reaction chamber. To confine this reactive stream, a mixture of hydrogen (10 sccm) and argon (290 sccm) was used as coaxial gas flow. Both precursor and coaxial flows intersect orthogonally with the infrared CO_2 laser beam (Rofin SCx30, λ = 10.6 μm) at 100 W power (Fig. 1a). In all the experiments the working pressure within the reaction chamber was fixed at 100 mbar. To capture and disperse nanoparticles, we used a liquid collection system where the exit stream was passed through a set of two bubblers containing dry and distilled 1-dodecene. The solvent colour changed to light yellow over time. Subsequently, the nanoparticle suspension was centrifuged and the light-yellow solid was washed with ethanol at 12 000 rpm for 20 minutes. The purification process was repeated 3 times to remove 1-dodecene excess. The nanoparticles can then be easily redispersed in different solvents (*e.g.* chloroform or ethanol). ^{1}H NMR ($CHCl_3$-d1) of 1-dodecene: δ = 5.78 (m, 1H, CH═), 5.00 (m, 2H, ═CH_2), 1.26 (m, 18H, CH_2), 0.85 (m, 3H, CH_3). ^{1}H NMR ($CHCl_3$-d1) of alkyl silicon nanoparticles: δ = 1.20 (m, 19H, CH_2), 0.75 (m, 6H, CH_3). IR of alkyl silicon nanoparticles: 2900–3000 ν C–H, 1450 δ C–H, 1259 δ (Si–)CH, 1015–1098 ν Si–O, 900 γ C–H, 796 ν Si–C. These experiments have been carried out in the Nanoparticle Synthesis Unit from the CIBER network.

Characterization methods

The obtained luminescent silicon nanoparticles were characterized through a battery of analytical methods. The particle morphology and size distribution were determined by using a FEI Tecnai transmission electron microscope (TEM) operated at 200 kV. At least, one hundred nanoparticles were evaluated to measure the mean diameter of the particles. High resolution transmission electron microscopy (HRTEM), scanning transmission electron microscopy with a high angle annular dark field detector (STEM-HAADF) and selected area electron diffraction (SAED) analysis were performed to determine the morphology and the crystalline structure, using a FEI Tecnai Field Emission Gun operated at 300 kV and a FEI Cs-image corrected (60–300 kV) TEM operated at 300 kV. Raman spectra were obtained with a Laser Raman WiTec Alpha 300 spectrometer, with the 532 nm line of an Ar+ ion laser. ^{1}H NMR spectra were obtained on a 300 MHz Bruker UltraShield™, after several centrifugations with ethanol as the antisolvent, followed by drying and redispersion in deuterated chloroform.

Fourier transform infrared spectroscopy (FTIR) was performed on a Bruker Vertex 70 FTIR spectrometer using the horizontal attenuated total reflectance (ATR) mode. Surface composition was analyzed by X-ray photoelectron spectroscopy (XPS) with an Axis Ultra DLD (Kratos Tech.). The spectra were excited by a monochromatic Al Kα source (1486.6 eV) run at 12 kV and 10 mA and pass energy of 20 eV was used. The binding energies were referenced to the internal C 1s (284.2 eV) standard. The optical properties were evaluated by fluorescence spectroscopy of the nanoparticle suspensions using an LS55 Fluorescence Spectrometer (PerkinElmer) equipped with a xenon arc lamp as the light source. The fluorescence quantum yield (QY) of silicon nanocrystal dispersion was determined by comparing the integrated photoluminescence intensities and the absorbance values of the Si nanocrystals with the reference quinine dye (QY of 54%).

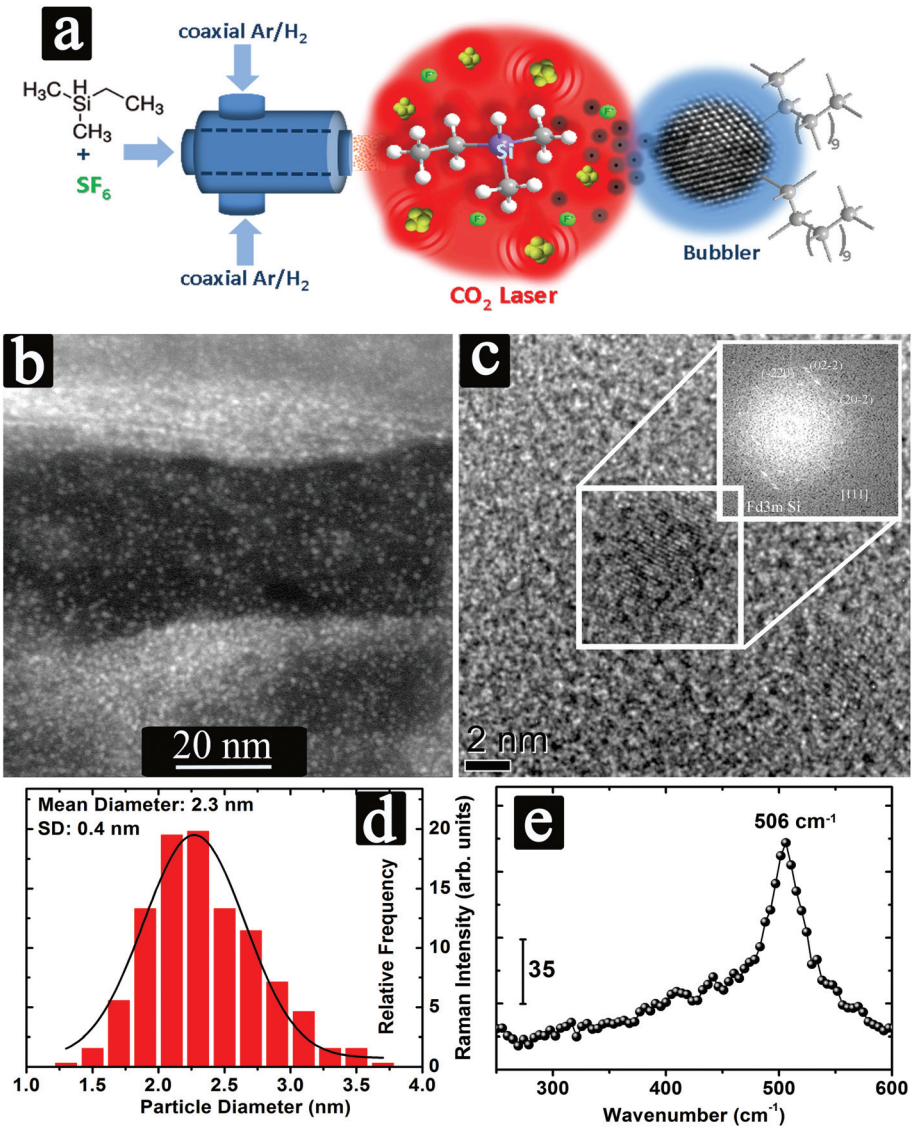

Fig. 1 Detail of the reaction area where the IR laser interacts with the reactants (a), STEM-HAADF (b), HRTEM image (c), size distribution (d) and Raman spectrum (e) of the as-prepared silicon nanocrystals.

Computational details

Periodic DFT computations were performed using the VASP package[34,35] with plane-wave basis sets and RPBE functional.[36–38] The cut-off energy used was 500 eV. All the results presented are the output of spin-polarized computations that were obtained by relaxing the structures until the net force acting on the ions was <0.015 eV $Å^{-1}$. The reaction paths were generated using the climbing image (CI-NEB) method.[39] A (111) cut was used for representing the surface of the silicon nanocrystals. We defined a p(1 × 1) rectangular slab that contains 32 Si atoms and is about 10 Å in height (8 layers). The vacuum height separating the periodic slabs is >11 Å. In the computations the 16 bottom Si atoms were kept fixed (4 layers), where all the remaining atoms were relaxed. The *k*-point sampling was generated by the Monkhorst–Pack procedure with a (3 × 3 × 1) mesh, for a 6.641 Å × 7.668 Å × 20.785 Å rectangular cell.

Results and discussion

Synthesis and characterization of the Si nanoparticles

In the laser pyrolysis method used in this work, the beam intersects the reactant stream containing the vapourized silicon precursor (dimethylethylsilane) and sulphur hexafluoride (SF_6), which is used as a photosensitizer, *i.e.* SF_6 absorbs energy from the laser source, transferring it to the reactant molecules. In the process, SF_6 dissociates to an extent that depends on the operating conditions (laser intensity and residence time).[32]

The gas stream containing the resulting Si nanocrystals is then dispersed in small bubbles through 1-dodecene. Collectively, these bubbles provide a large interfacial area that acts as an effective sink for the nanocrystals formed, and also for any other species amenable to liquid phase absorption.

Fig. 1b shows a STEM-HAADF image (the contrast depends directly on the atomic number Z^2), where the bright Si nanoparticles are easily spotted against the C layer of the grid and the solvent. The nanocrystals appear as well-dispersed spherical particles.

The size distribution of the silicon nanocrystals determined by TEM is displayed in Fig. 1d indicating that the mean diameter is 2.3 nm with a standard deviation of 0.4 nm. Agglomerates were largely absent in the observations of the collected product. Moreover, the lattice planes of 0.19 nm corresponding to (220) plane spacing in the HRTEM image (Fig. 1c) demonstrate the *Fd3m* crystalline structure of the as-prepared silicon nanocrystals.[13,32,40]

Raman spectroscopy of the as-prepared Si nanocrystals is presented in Fig. 1e. The transverse optical (TO) mode downshifts to 505–507 cm^{-1} in comparison with the peak position of single crystalline bulk Si centered at 521 cm^{-1}. This downshift to lower wave-number values accompanied by an asymmetrical broadening of the Raman spectrum can be attributed to the presence of additional phonon modes that become active beyond the Brillouin zone with decreasing nanocrystal sizes.[41,42] According to theoretical predictions, the peak position corresponds to crystalline sizes below 3 nm, in good agreement with the size distributions observed by TEM inspection (Fig. 1d). Moreover, the presence of surface distortions[43,44] and/or the formation of hexagonal (wurtzite-type) phases can also explain in part this downshift in the main peak position.[45–49] HR-TEM further suggests the existence of the $P6_3mc$ hexagonal phase for a considerable number of indexed nanoparticles (see the ESI†).

These observations indicate that the synthesis method used here produces well-dispersed Si particles where a combination of cubic and hexagonal crystalline phases appears to be present. The characteristics of the surface ligands were further studied by ^{1}H NMR and FTIR techniques. The ^{1}H NMR spectrum of the silicon nanocrystals is shown in Fig. 2a (bottom spectrum). For this measurement, the colloid was dried out under vacuum and redispersed in deuterated chloroform ($CHCl_3$-d1). The ^{1}H-NMR spectrum of the 1-dodecene (Fig. 2a, upper spectrum) shows the resonance of the terminal vinylic protons ($=CH_2$) and the internal olefinic proton (–CH=) at δ 5.00 and δ 5.78 respectively. The methylene proton ($–CH_2–$) and methyl proton ($–CH_3$) resonances are displayed downfield (δ 1.26 and δ 0.85, respectively). In comparison with pure 1-dodecene, the alkyl-capped silicon nanoparticles (Fig. 2a, bottom spectrum) show no resonance in the range δ 6.0–5.0 confirming the absence of olefinic terminal protons.

The absence of high-field signals from the olefinic protons is the most relevant feature of the spectrum and strongly suggests that the hydrosilylation reaction has taken place. In contrast, signals at δ 1.20 corresponding to the CH_2 and CH protons and δ 0.75 to the methyl groups (CH_3), remain without a significant change. The integration of these two signals results in 19H ($–CH_2–$ and –CH–) and 6H ($–CH_3$). This indicates that the hydrosilylation reaction yields *sec*-alkyl silicon

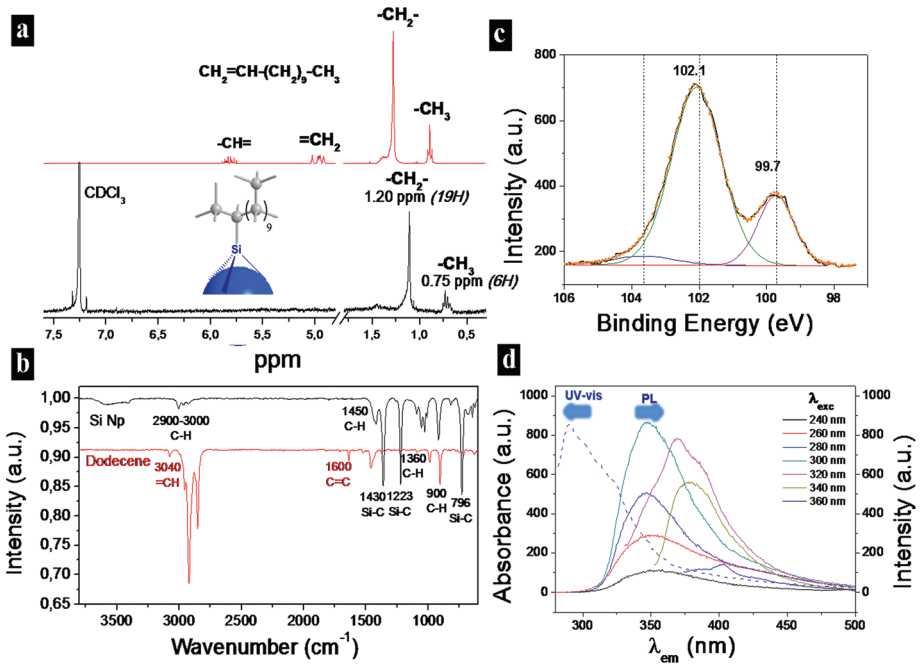

Fig. 2 ^{1}H NMR spectrum (a), FTIR spectrum (b), XPS spectrum (c) and UV-Vis absorbance spectrum (dashed line), and emission spectra (solid lines) at different excitation wavelengths (d) of the alkyl-capped silicon nanocrystals.

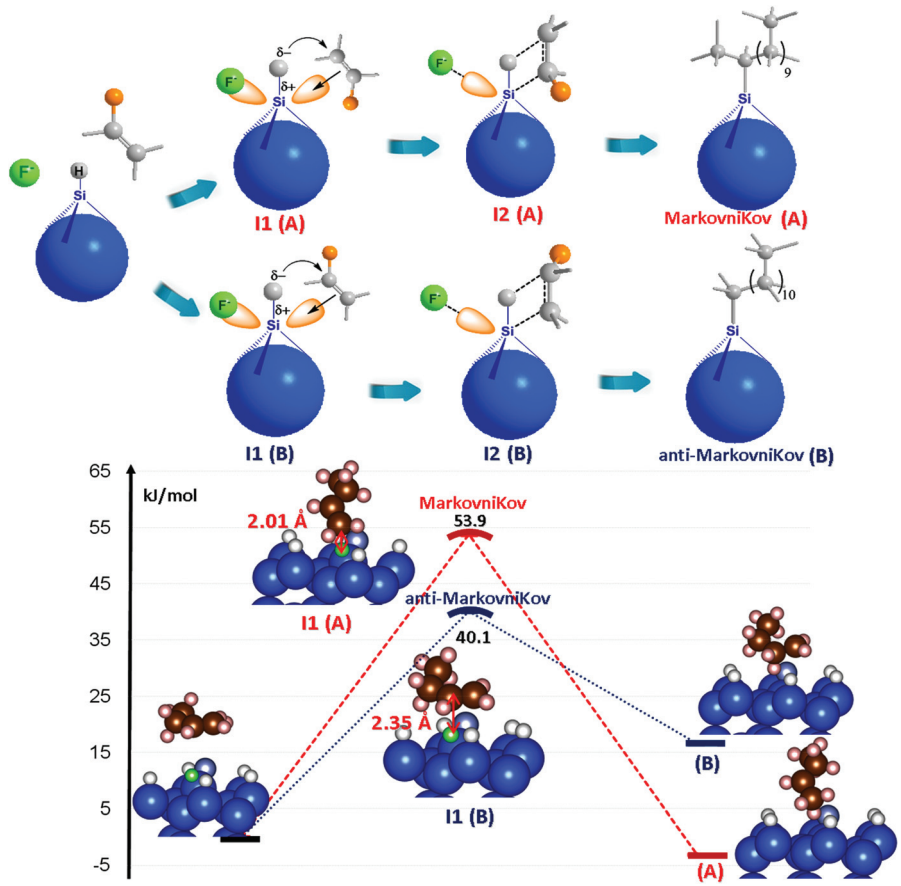

Fig. 3 Fluoride-assisted mechanism proposed for room temperature hydrosilylation and DFT calculations for the competing Markovnikov or anti-Markovnikov hydrosilylation mechanism at room temperature.

substituted (Si-CHMe-R) surface groups exclusively, following a Markovnikov addition-mechanism (Fig. 3).

These alkylated Si NPs have been further characterized by IR spectroscopy (Fig. 2b). The original solvent was removed and the Si nanocrystals were dispersed in ethanol. The FTIR spectrum of silicon nanocrystals in Fig. 2b (upper spectrum) reveals the presence of an organic layer as noted by the Csp_3–H stretching bands between 2900 and 3000 cm^{-1},[13,22] as well as the C–H vibration modes at 1450 cm^{-1} and 900 cm^{-1} corresponding to the bending modes of the CH_2 and CH_3 groups.[17] The absorption bands at 1259 cm^{-1} and 796 cm^{-1} correspond to Si–C vibration modes,[13,14,17] confirming the covalent bonding of 1-dodecene to the surface of the particles. The broad absorption in the range 1095–1015 cm^{-1} is assigned to a Si–O–Si species that most likely form under ambient exposure. The absence of the stretching bands corresponding to the double bond (=CH and C=C) of 1-dodecene (Fig. 2b, bottom spectrum) in the ranges 3040–3010 and 1690–1620 cm^{-1}, in the FTIR spectrum of the silicon nanocrystals again indicates that hydrosilylation has taken place.

Further confirmation of the Si–C bonding was obtained from X-ray photoelectron spectroscopy (XPS) carried out on as-prepared nanoparticles (Fig. 2c). High-resolution scanning of the Si 2p region shows two main peaks at 99.7 and 102.1 eV. The binding energy observed at 102.1 eV is assigned to Si–C bonds[50,51] from the covalent bonding between the alkyl chains and the silicon surface. The enrichment of the outer surface of the Si NPs with randomly distributed C atoms has also been suggested in previous reports and it might be additional contribution to this band.[52] Likewise, the peak at 99.7 eV is attributed to elemental silicon.[22,53] The small shoulder at 103.5 eV also indicates some incipient oxidation of the Si nanoparticles.[22] It is remarkable, however, that in spite of their small size, the extent of this oxidation is almost negligible. The optical properties of the alkyl-capped silicon nanocrystals were studied by UV-Vis and fluorescence spectroscopy.

Fig. 2d presents the UV-Vis absorbance and photoluminescence (PL) measurements performed on dispersions of the nanoparticles in hexane. The emission spectra of the as-prepared Si NP colloid were collected at excitation wavelengths ranging from 240 to 360 nm in 20 nm intervals. As a control, the absence of luminescence was checked with two samples, a hexane solution of a precursor and a hexane solution of distilled 1-dodecene. The PL peak of the alkyl-capped silicon nanocrystals shifted from 340 to 400 nm as the excitation wavelength increased, reaching a PL maximum emission at 350 nm

when excited at 300 nm. However, the PL intensity decreased as the PL peak red-shifted. This behaviour is in good agreement with previous reports on luminescence values for alkyl-functionalized oxide-free silicon[14,22,25,54] and can be attributed to the Γ–Γ direct band gap transitions.[5,26] However in our case the emission range is very narrow (FWHM = 70 nm), reflecting the narrow size distribution of the sample,[22] in contrast to broader emission bands attributed to size polydispersity.[13,14,24,55] The quantum yield (QY) of the alkyl-coated silicon nanocrystals was estimated to be 6.5%, comparable to previously reported QY values.[56,57]

To prove that silicon nanoparticles were formed in the reaction zone, a control experiment was performed by collecting the freshly nucleated particles directly into a bubbler containing dodecene without previous deaeration and distillation treatment. Under less strict anhydrous conditions, non-luminescent silicon oxide nanoparticles were obtained, suggesting that silicon nanoparticles that are prone to oxidation are preferentially formed in spite of the Si/C ratio of the initial DMES precursor. The presence of silicon carbide (SiC) nanoparticles could be anticipated in view of the initial stoichiometry of the silicon precursor. Moreover, given the intrinsic stability typically attributed to SiC NPs,[9,58] a permanent luminescence response should have been obtained regardless of the deaeration degree of the tested solvents (dodecene and alternatively ethylene glycol). Nevertheless, only quenched oxidized nanoparticles could be detected under our experimental conditions (data not shown). It is also worth mentioning that analogous alkyl–silane precursors with high carbon content (*i.e.* diphenyl silane) have been previously reported to yield brightly luminescent silicon nanocrystals synthesized under supercritical conditions in the presence of high-boiling organic solvents.[5]

Additional control experiments were also carried out to corroborate the crucial role of fluoride species on the silylation at room temperature in our collecting system.[59,60] First of all, SF_6 flow was deliberately excluded from the gas flow to discard the fluoride input from the sensitizer upon laser decomposition. The production of nanoparticles after laser pyrolysis of DMES was still achieved at different laser power intensities even in the absence of a sensitizer gas (SF_6). Similar to the most widespread reported silicon precursor SiH_4, DMES could be decomposed under laser irradiation but without incurring the security limitations of the former. Nevertheless, these nanoparticles were not successfully hydrosilylated and showed a clear tendency to oxidation and quenching over time. A final and concluding experiment was carried out by the addition of a catalytic amount of $EtAlCl_2$ in hexane (1 M, 0.5 mL) to the 1-dodecene in the collection vessel. This experiment was analogous to the previous ones and SF_6 was not present in the gas stream. In this latter case though, a blue-emitting solution containing Si NPs was obtained. The Lewis acid catalyst led to the successful passivation of the newly formed nanoparticles (data not shown) at room temperature as expected from previous reports.[61,62] This last experiment further corroborated two facts: (i) the formation of non-oxidized silicon nanoparticles by laser pyrolysis of DMES without the necessity of an IR-absorber and (ii) the capacity of fluoride anions from SF_6 decomposition to mediate as catalytic species for room temperature hydrosilylation of Si NPs.[59,60]

Reaction mechanism

The discussed results provide a strong evidence of the room temperature hydrosilylation between 1-dodecene and the entrained Si nanoparticles. We have also shown that the reaction produces *sec*-alkyl silicon substituted (Si-CHMe-R) surface groups exclusively, following a Markovnikov addition mechanism. To explain this, we propose a mechanism mediated by the fluoride species[59,60] originating on SF_6 decomposition,[32] where the first step corresponds to a nucleophilic attack of fluoride ions resulting in pentavalent intermediates[59,60] **I1(A)** and **I1(B)** (Fig. 3), which could then transfer a hydride (H^-) to the double bond through four-center intermediates **I2(A)** and **I2(B)** facilitating Si–C bond formation, as illustrated in Fig. 3.

While two possible regioisomers exist corresponding to Markovnikov (**A**) or anti-Markovnikov (**B**) addition (Fig. 3), the ^{1}H-RMN data correlate well with perfect regioselectivity of 100% Markovnikov addition (Fig. 2a).

Theoretical calculations have been carried out in order to clarify the directing factors that control this regioselective reaction pathway. Fig. 3 shows the calculated energy diagram for the Markovnikov (**A**) and competing anti-Markovnikov (**B**) addition. It can be seen that the activation energy favors the anti-Markovnikov hydrogenation with a barrier of 40.1 kJ mol^{-1} *versus* 53.9 kJ mol^{-1} for the Markovnikov addition. However, the Markovnikov mechanism is thermodynamically favoured. The anti-Markovnikov hydrosilylation results in a relatively unstable structure prone to dehydrogenation with an estimated barrier of 23.4 kJ mol^{-1}. Our calculations reveal that the anti-Markovnikov hydrosilylation is endothermic by 16.7 kJ mol^{-1} *versus* a slightly exothermic, −3.1 kJ mol^{-1}, Markovnikov path (see Fig. 3). Even though the ease of silicon functionalization in solution is well documented in the literature,[63] there are not many examples reported for analogous processes dealing with the surface chemistry of silicon nanoparticles. Stabilization and protection of freshly formed Si nanoparticles from oxidation is especially relevant. Given their small size even a moderate degree of surface oxidation would strongly decrease the proportion of silicon.

The approach proposed here relies on the room temperature surface functionalization of silicon nanoparticles through the fluoride-intermediate mechanism as the most viable hydrosilylation route. In our opinion, this seems to be also the most probable reaction pathway in the recent work by Yixuan Yu *et al.*[40] that claimed a room temperature hydrosilylation step catalyzed by ester or carboxylic groups. In their particular experimental conditions, the presence of fluoride ions from the preliminary acid etching step is quite plausible. Likewise, the polar character of the C–O would preferentially facilitate the hydride transfer from the silicon center to the electrophilic carbon to yield the corresponding alkoxide. Moreover, the strategy proposed here offers several advantages compared to previous reports on synthesis of silicon nanoparticles assisted

by laser[28,29] or non-thermal plasma[30] since we substitute the highly toxic silane precursor by a safer one that does not require special conditioning and we do not perform additional post-treatments for etching of undesired crystalline phases or critical adjustment of nanoparticle size.[11,28]

Conclusions

We have developed a facile and room temperature route for the continuous production of light-emitting silicon nanoparticles. This safe and convenient method combines laser pyrolysis of a tri-alkyl silicon precursor (instead of the highly toxic and flammable SiH_4 that is customarily used as a silicon source) and a one-step collection and stabilization of the produced nanoparticles. This strategy represents a significant improvement with respect to previous results by laser pyrolysis that required acid etching post-treatment. In our case, both the use of an unsaturated solvent as a liquid medium to collect the nanocrystals and SF_6 as a laser sensitizer gas are key experimental parameters that allow further organic functionalization without any pre- or post-treatment. On the other hand, we have proposed a fluoride assisted hydrosilylation mechanism which is responsible for the regioselective reaction pathway as further demonstrated by DFT calculations. Therefore, this synthesis strategy constitutes a superior alternative regarding conventional laser pyrolysis of SiH_4.

Acknowledgements

Financial support from MINECO (Spain) is gratefully acknowledged. CIBER-BBN is an initiative funded by the VI National R&D&i Plan 2008–2011, Iniciativa Ingenio 2010, Consolider Program, CIBER Actions and financed by the Instituto de Salud Carlos III with assistance from the European Regional Development Fund. The microscopy work was conducted in the "Laboratorio de Microscopias Avanzadas" at "Instituto de Nanociencia de Aragon – Universidad de Zaragoza. JLH acknowledges a "Juan de la Cierva" Postdoctoral Fellowship and a Marie Curie Reintegration Grant (NANOLIGHT-294094). Authors thank Dr Silvia Irusta for many helpful discussions and for performing the XPS measurements.

Notes and references

1 S. Godefroo, M. Hayne, M. Jivanescu, A. Stesmans, M. Zacharias, O. I. Lebedev, G. Van Tendeloo and V. V. Moshchalkov, *Nat. Nanotechnol.*, 2008, **3**, 174–178.
2 N. Koshida, *Device Applications of Silicon Nanocrystals and Nanostructures*, Springer, 2009.
3 F. Peng, Y. Y. Su, Y. L. Zhong, C. H. Fan, S. T. Lee and Y. He, *Acc. Chem. Res.*, 2014, **47**, 612–623.
4 Z. F. Ding, B. M. Quinn, S. K. Haram, L. E. Pell, B. A. Korgel and A. J. Bard, *Science*, 2002, **296**, 1293–1297.
5 J. D. Holmes, K. J. Ziegler, R. C. Doty, L. E. Pell, K. P. Johnston and B. A. Korgel, *J. Am. Chem. Soc.*, 2001, **123**, 3743–3748.
6 N. H. Alsharif, C. E. M. Berger, S. S. Varanasi, Y. Chao, B. R. Horrocks and H. K. Datta, *Small*, 2009, **5**, 221–228.
7 J. H. Park, L. Gu, G. von Maltzahn, E. Ruoslahti, S. N. Bhatia and M. J. Sailor, *Nat. Mater.*, 2009, **8**, 331–336.
8 L. P. a. R. Tura, *Silicon Nanocrystals: Fundamentals, Synthesis and Applications*, WILEY-VCH Verlag GmbH & Co. KGaA, Weinheim, Germany, 2010.
9 J. Y. Fan and P. K. Chu, *Small*, 2010, **6**, 2080–2098.
10 J. P. Wilcoxon, G. A. Samara and P. N. Provencio, *Phys. Rev. B: Condens. Matter*, 1999, **60**, 2704–2714.
11 R. Intartaglia, K. Bagga, F. Brandi, G. Das, A. Genovese, E. Di Fabrizio and A. Diaspro, *J. Phys. Chem. C*, 2011, **115**, 5102–5107.
12 R. Intartaglia, A. Barchanski, K. Bagga, A. Genovese, G. Das, P. Wagener, E. Di Fabrizio, A. Diaspro, F. Brandi and S. Barcikowski, *Nanoscale*, 2012, **4**, 1271–1274.
13 N. Shirahata, M. R. Linford, S. Furumi, L. Pei, Y. Sakka, R. J. Gates and M. C. Asplund, *Chem. Commun.*, 2009, 4684–4686.
14 D. Z. Tan, Z. J. Ma, B. B. Xu, Y. Dai, G. H. Ma, M. He, Z. M. Jin and J. R. Qiu, *Phys. Chem. Chem. Phys.*, 2011, **13**, 20255–20261.
15 D. Z. Tan, B. B. Xu, P. Chen, Y. Dai, S. F. Zhou, G. H. Ma and J. R. Qiu, *RSC Adv.*, 2012, **2**, 8254–8257.
16 Y. He, Y. L. Zhong, F. Peng, X. P. Wei, Y. Y. Su, S. Su, W. Gu, L. S. Liao and S. T. Lee, *Angew. Chem., Int. Ed.*, 2011, **50**, 3080–3083.
17 A. S. Heintz, M. J. Fink and B. S. Mitchell, *Adv. Mater.*, 2007, **19**, 3984–3988.
18 V. Amendola and M. Meneghetti, *Phys. Chem. Chem. Phys.*, 2013, **15**, 3027–3046.
19 A. S. Heintz, M. J. Fink and B. S. Mitchell, *Appl. Organomet. Chem.*, 2010, **24**, 236–240.
20 K. Abderrafi, R. G. Calzada, M. B. Gongalsky, I. Suarez, R. Abarques, V. S. Chirvony, V. Y. Timoshenko, R. Ibanez and J. P. Martinez-Pastor, *J. Phys. Chem. C*, 2011, **115**, 5147–5151.
21 V. Sebastian, M. Arruebo and J. Santamaria, *Small*, 2014, **10**, 835–853.
22 M. Rosso-Vasic, E. Spruijt, B. van Lagen, L. De Cola and H. Zuilhof, *Small*, 2008, **4**, 1835–1841.
23 J. H. Warner, A. Hoshino, K. Yamamoto and R. D. Tilley, *Angew. Chem., Int. Ed.*, 2005, **44**, 4550–4554.
24 B. A. Manhat, A. L. Brown, L. A. Black, J. B. A. Ross, K. Fichter, T. Vu, E. Richman and A. M. Goforth, *Chem. Mater.*, 2011, **23**, 2407–2418.
25 J. Wang, S. Q. Sun, F. Peng, L. X. Cao and L. F. Sun, *Chem. Commun.*, 2011, **47**, 4941–4943.
26 A. Shiohara, S. Hanada, S. Prabakar, K. Fujioka, T. H. Lim, K. Yamamoto, P. T. Northcote and R. D. Tilley, *J. Am. Chem. Soc.*, 2010, **132**, 248–253.
27 F. J. Hua, M. T. Swihart and E. Ruckenstein, *Langmuir*, 2005, **21**, 6054–6062.

28 X. G. Li, Y. Q. He, S. S. Talukdar and M. T. Swihart, *Langmuir*, 2003, **19**, 8490–8496.
29 M. T. Swihart, *Curr. Opin. Colloid Interface Sci.*, 2003, **8**, 127–133.
30 L. Mangolini and U. Kortshagen, *Adv. Mater.*, 2007, **19**, 2513–2519.
31 L. Mangolini, E. Thimsen and U. Kortshagen, *Nano Lett.*, 2005, **5**, 655–659.
32 A. Malumbres, G. Martinez, R. Mallada, J. L. Hueso, O. Bomati-Miguel and J. Santamaria, *Nanotechnology*, 2013, **24**, 325603.
33 G. Martinez, A. Malumbres, R. Mallada, J. L. Hueso, S. Irusta, O. Bomati-Miguel and J. Santamaria, *Nanotechnology*, 2012, **23**, 425605.
34 G. Kresse and J. Hafner, *Phys. Rev. B: Condens. Matter*, 1994, **49**, 14251–14269.
35 A. Vojta, Q. Z. Wen and D. R. Clarke, *Comput. Mater. Sci.*, 1996, **6**, 51–62.
36 P. E. Blochl, *Phys. Rev. B: Condens. Matter*, 1994, **50**, 17953–17979.
37 B. Hammer, L. B. Hansen and J. K. Norskov, *Phys. Rev. B: Condens. Matter*, 1999, **59**, 7413–7421.
38 J. P. Perdew, J. A. Chevary, S. H. Vosko, K. A. Jackson, M. R. Pederson, D. J. Singh and C. Fiolhais, *Phys. Rev. B: Condens. Matter*, 1992, **46**, 6671–6687.
39 G. Henkelman, B. P. Uberuaga and H. Jonsson, *J. Chem. Phys.*, 2000, **113**, 9901–9904.
40 Y. Yu, C. M. Hessel, T. D. Bogart, M. G. Panthani, M. R. Rasch and B. A. Korgel, *Langmuir*, 2013, **29**, 1533–1540.
41 G. Faraci, S. Gibilisco, A. R. Pennisi and C. Faraci, *J. Appl. Phys.*, 2011, **109**, 074311.
42 H. Richter, Z. P. Wang and L. Ley, *Solid State Commun.*, 1981, **39**, 625–629.
43 H. Xia, Y. L. He, L. C. Wang, W. Zhang, X. N. Liu, X. K. Zhang, D. Feng and H. E. Jackson, *J. Appl. Phys.*, 1995, **78**, 6705–6708.
44 V. Petkov, C. M. Hessel, J. Ovtchinnikoff, A. Guillaussier, B. A. Korgel, X. F. Liu and C. Giordano, *Chem. Mater.*, 2013, **25**, 2365–2371.
45 J. Bandet, B. Despax and T. Caumont, *J. Phys. D: Appl. Phys.*, 2002, **35**, 234–239.
46 A. F. I. Morral, J. Arbiol, J. D. Prades, A. Cirera and J. R. Morante, *Adv. Mater.*, 2007, **19**, 1347–1351.
47 J. D. Prades, J. Arbiol, A. Cirera, J. R. Morante and A. F. I. Morral, *Appl. Phys. Lett.*, 2007, **91**, 123107.
48 F. J. Lopez, U. Givan, J. G. Connell and L. J. Lauhon, *ACS Nano*, 2011, **5**, 8958–8966.
49 F. J. Lopez, E. R. Hemesath and L. J. Lauhon, *Nano Lett.*, 2009, **9**, 2774–2779.
50 A. Avila, I. Montero, L. Galan, J. M. Ripalda and R. Levy, *J. Appl. Phys.*, 2001, **89**, 212–216.
51 E. J. Henderson, C. M. Hessel and J. G. C. Veinot, *J. Am. Chem. Soc.*, 2008, **130**, 3624–3632.
52 C. E. Rowland, D. C. Hannah, A. Demortiere, J. H. Yang, R. E. Cook, V. B. Prakapenka, U. Kortshagen and R. D. Schaller, *ACS Nano*, 2014, **8**, 9219–9223.
53 C. M. Hessel, M. R. Rasch, J. L. Hueso, B. W. Goodfellow, V. A. Akhavan, P. Puvanakrishnan, J. W. Tunnel and B. A. Korgel, *Small*, 2010, **6**, 2026–2034.
54 R. D. Tilley, J. H. Warner, K. Yamamoto, I. Matsui and H. Fujimori, *Chem. Commun.*, 2005, 1833–1835.
55 H. T. Li, X. D. He, Z. H. Kang, H. Huang, Y. Liu, J. L. Liu, S. Y. Lian, C. H. A. Tsang, X. B. Yang and S. T. Lee, *Angew. Chem., Int. Ed.*, 2010, **49**, 4430–4434.
56 F. Erogbogbo, K. T. Yong, I. Roy, G. X. Xu, P. N. Prasad and M. T. Swihart, *ACS Nano*, 2008, **2**, 873–878.
57 C. M. Hessel, E. J. Henderson and J. G. C. Veinot, *Chem. Mater.*, 2006, **18**, 6139–6146.
58 M. C. Ortega-Liebana, J. L. Hueso, R. Arenal, R. Lahoz, G. F. De la Fuente and J. Santamaria, *J. Phys. Chem. C*, 2015, **119**, 2158–2165.
59 J. M. Buriak, *Chem. Rev.*, 2002, **102**, 1271–1308.
60 R. Boukherroub, S. Morin, D. D. M. Wayner, F. Bensebaa, G. I. Sproule, J. M. Baribeau and D. J. Lockwood, *Chem. Mater.*, 2001, **13**, 2002–2011.
61 J. M. Buriak and M. J. Allen, *J. Am. Chem. Soc.*, 1998, **120**, 1339–1340.
62 F. Zipoli and M. Bernasconi, *J. Phys. Chem. B*, 2006, **110**, 23403–23409.
63 R. J. P. Corriu, C. Guerin and J. J. E. Moreau, *Top. Stereochem.*, 1984, **15**, 43–198.